

RT-CW, widely tunable semiconductor THz QCL sources

M. Razeghi* and Q. Y. Lu

Center for Quantum Devices, Department of Electrical Engineering and Computer Science, Northwestern University, Evanston, IL 60208, USA.

razeghi@eecs.northwestern.edu

ABSTRACT

Distinctive position of Terahertz (THz) frequencies ($\square\sim 0.3$ -10 THz) in the electromagnetic spectrum with their lower quantum energy compared to IR and higher frequency compared to microwave range allows for many potential applications unique to them. Especially in the security side of the THz sensing applications, the distinct absorption spectra of explosives and related compounds in the range of 0.1–5 THz makes THz technology a competitive technique for detecting hidden explosives. A compact, high power, room temperature continuous wave terahertz source emitting in a wide frequency range will greatly boost the THz applications for the diagnosis and detection of explosives. Here we present a new strong-coupled strain-balanced quantum cascade laser design for efficient THz generation based intracavity DFG. Room temperature continuous wave operation with electrical frequency tuning range of 2.06-4.35 THz is demonstrated.

Keywords: terahertz, Terahertz source, quantum cascade lasers, difference frequency generation, continuous wave operation, monolithic tuning

1. INTRODUCTION

THz sources based on intracavity difference frequency generation (DFG) in mid-IR QCLs are currently the only semiconductor light source that emits over 1-5 THz range with optical power up to mW at room temperature.[1] When a QCL active region is designed with strong coupling between the lower lasing levels and injector levels, which results in a large nonlinear susceptibility $\square^{(2)}$, THz emission can be generated within the cavity [2]. Thus, this type of THz source is free from the temperature limitation suffered by the THz QCLs based on direct optical transition, and ideally its working temperature is only limited by the mid-IR QCL which can work well even above 100 \square C [3], and can be tuned over a broad waveguide range with broadband heterogeneous active region design [4]. It not only shares the common features of the mid-IR QCLs which are mass reproducible, room temperature operation, low cost, compact size, and high efficiency, but also carries the potential of delivering THz emission with high power in a wide frequency range.

With the recent systematic optimizations, including dual-core design based on single phonon resonance structure [5] for high efficiency and broad gain operation, use of a composite distributedfeedback (DFB) grating with dual period component [2] for purifying and tuning the mid-IR as well as the THz spectra, and use of the epi-down Čerenkov phase-matching scheme [6] for high THz outcoupling efficiency, THz sources based on DFG in QCLs with high THz power up to 1.9 mW [1], and wide tuning range of 1-4.6 THz have been demonstrated [5,7], as summarized in Figure 1. Very recently, by utilizing a low-loss buried-ridge waveguide design and highly dissipative epi-down mounting scheme, room temperature continuous wave (RT-CW) operation at 3.6 THz was demonstrated with a continuous power of 3 \square W. [8] Room temperature monolithic THz tuning of 2.64.2 THz from a sampled-grating distributed feedback distributed Bragg (SGDFB-DBR) QCL device is also demonstrated. [9] While this narrowband THz source is suitable as a local oscillator for

heterodyne detections in space observatories, continuous wave, monolithic THz frequency tuning with higher power is always desired for real applications such as chemical sensing and spectroscopy.

Terahertz Emitters, Receivers, and Applications VII, edited by Manijeh Razeghi, Alexei N. Baranov, John M. Zavada, Dimitris Pavlidis, Proc. of SPIE Vol. 9934, 993406 · © 2016 SPIE
 CCC code: 0277-786X/16/\$18 · doi: 10.1117/12.2240398

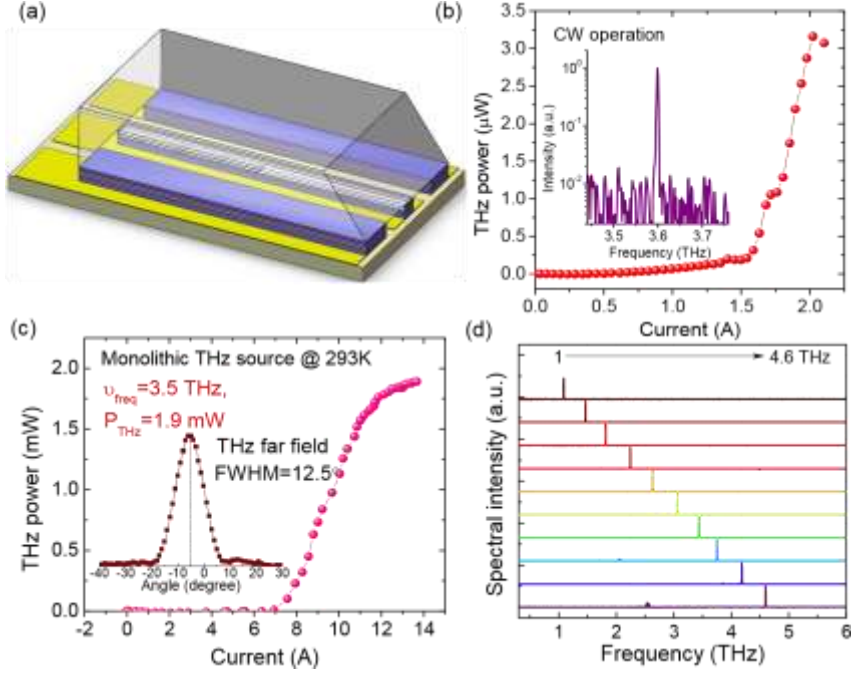


Figure 1. Recent development of THz QCL sources based on DFG.

2. DESIGN OF STRAIN-BALANCED QCL ACTIVE REGION FOR THz DFG

To further enhance the CW THz performance, we present a new strong-coupled strain-balanced quantum cascade laser design for efficient THz generation based intracavity DFG [10]. The band structure is shown in Figure 2. The targeted wavelength is $\lambda \sim 7.8 \text{ } \mu\text{m}$. The inserted $\text{Ga}_{0.47}\text{In}_{0.53}\text{As}$ layers are used to balance the material strain within one stage. The conduction band offset is enhanced to $\sim 0.74 \text{ eV}$. In the present strain-balanced design with a diagonal optical transition scheme, the increased conduction-band offset and interface roughness increases the broadening the oscillation linewidth to $\sim 15\text{-}20 \text{ meV}$, compared to that of $\sim 10 \text{ meV}$ for the lattice-matched active region design [5]. This allows for a stronger coupling design between the injector and upper lasing level. A high coupling strength with an energy splitting of $2\hbar\omega = 16.5 \text{ meV}$ is calculated for the present structure. This strong-coupling design not only effectively improves the carrier tunnelling rate into the upper lasing level 5, but also enhances the DFG nonlinear susceptibility $\chi^{(2)}$. The strong-coupling design with an energy splitting of 16.5 meV , provides another scheme to the total nonlinear susceptibility. Given a threshold gain $g_{th} = 5 \text{ cm}^{-1}$ (considering a waveguide loss of 1.2 cm^{-1} and mirror loss of 1.8 cm^{-1} for a 4-mm long cavity with high-reflection (HR) coating, and modal confinement factor of 60%), transition broadening $\Delta E = 15 \text{ meV}$ and 5 meV for the mid-IR transitions and THz transitions, a total nonlinear susceptibility of $|\chi^{(2)}| = 2.0 \times 10^4$ is obtained from the present design.

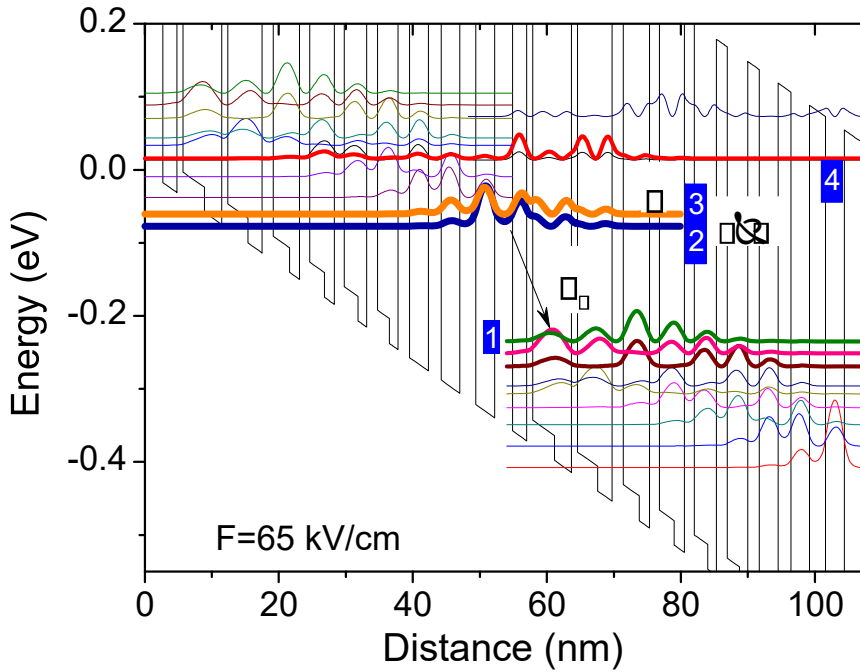


Figure 2 Active region band structure for the strain-balanced $\text{Al}_{0.63}\text{In}_{0.37}\text{As}/\text{Ga}_{0.35}\text{In}_{0.65}\text{As}/\text{Ga}_{0.47}\text{In}_{0.53}\text{As}$ material system design.

3. MID-IR AND THZ POWER PERFORMANCES

The other benefit of this strong-coupled strain-balanced design is the increased gain spectral width compared to the lattice matched design. The electroluminescence (EL) spectrum measured from a 40-stage single-core strain-balanced structure grown on an n-InP substrate exhibits a full-width at half maximum (FWHM) of 380 cm^{-1} (shown in Figure 3(a)). This is even broader than the previous dual-core lattice-matched active region with a FWHM of $\sim 330 \text{ cm}^{-1}$ in the $9\text{-}11 \text{ } \mu\text{m}$ wavelength range. The increased FWHM of EL spectra is attributed to the strong-coupled diagonal optical transition design involving multiple transitions and the increased oscillation linewidths. This single-core strain-balanced design is thus able to support 1-5 THz composite DFB designs with the designed wavelengths within 90% of the EL peak, as indicated by shaded area in Figure 3(a).

In the experiment, a laser structure consisting of 40 stages of strain-balanced structure was grown on a semi-insulating InP substrate. The molecular beam epitaxy growth started with a 200-nm InGaAs layer (Si, $\sim 1 \times 10^{18} \text{ cm}^{-3}$), and $3\text{-}\mu\text{m}$ InP buffer layer (Si, $\sim 2 \times 10^{16} \text{ cm}^{-3}$). After the active region growth with an average doping of $\sim 2.1 \times 10^{16} \text{ cm}^{-3}$, the growth ended with a 400-nm-thick InGaAs grating layer (Si, $\sim 2 \times 10^{16} \text{ cm}^{-3}$) and a 10-nm-thick InP cladding layer (Si, $\sim 2 \times 10^{16} \text{ cm}^{-3}$). Part of this wafer was processed into buried-compositeDFB, buried-ridge waveguides with double-side current extraction schemes following the procedure described in Refs. 6 and 8, while the other part of the wafer without grating patterns was processed into Fabry-Pérot (FP) devices for comparison. Grating periods of

$\square_1=1.18 \text{ } \mu\text{m}$ and $\square_2=1.30 \text{ } \mu\text{m}$ were used for the two components of the composite-DFB grating design. The wafer was regrown with $4.5\text{-}\mu\text{m}$ InP cladding (Si, $2\text{-}5 \times 10^{16} \text{ cm}^{-3}$) and

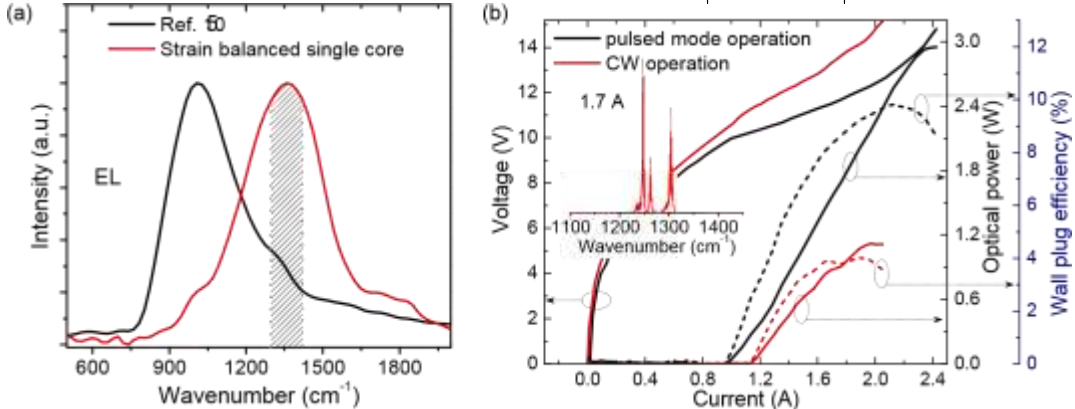


Figure 3 (a) EL spectra for the strain-balanced single-core design and the lattice matched dual-core design from Ref. 5. The shaded area indicates the supported dual wavelength emissions with the frequency spacing up to 5 THz. (b) *P-I-V* and wall plug efficiency characterizations of a 4.9-mm long uncoated FP device in pulsed mode and CW operations at 293 K. Inset: lasing spectrum at 1.7 A in CW operation.

0.5- μ m InP (Si, 5×10^{18} cm⁻³) cap layers on the grating layer by metal organic chemical vapor phase deposition (MOCVD). The front facet of the composite DFB device was polished into 30 μ to collect the THz light satisfying the Čerenkov phase matching condition. The DFB and FP devices were epi-down mounted on diamond submounts predefined with corresponding Indium patterns for efficient heat extraction

Figure 2(b) is the optical power-current-voltage (*P-I-V*) characterizations of a 12- μ m wide, 4.9-mm long, uncoated FP device on a semi-insulating substrate in pulsed mode (pulse width=200 ns and duty cycle=2%) and CW operations at 293 K. The inset is the CW lasing spectrum at 1.7 A. The FP device exhibits a maximum power of 3 W and threshold current density of 1.95 kA/cm² in pulsed mode operation, and a maximum power of 1.1 W and a threshold current density of 2.2 kA/cm² in CW operation. The maximum wall plug efficiencies (WPEs) are 10% and 4% for pulsed mode and CW operations, respectively. This is compared with previous results based on latticed matched active region with maximum

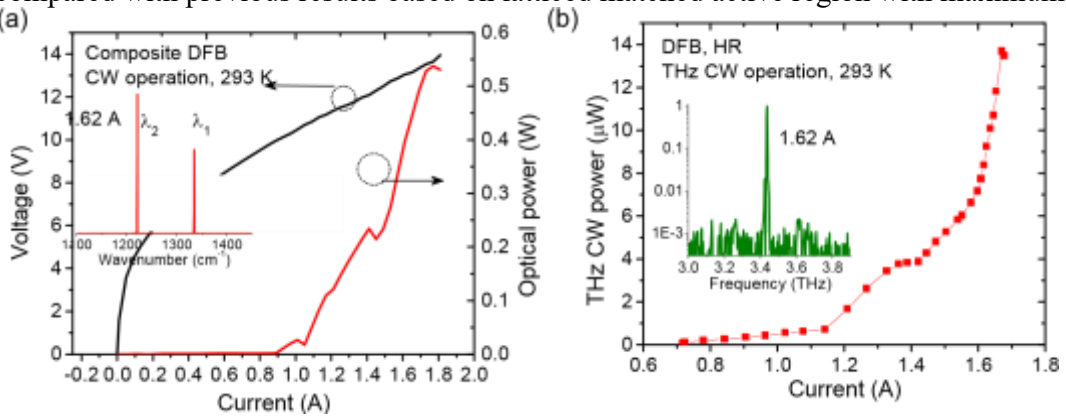


Figure 4 (a) *P-I-V* characterizations of a 4-mm long buried-ridge composite DFB device in CW operations at 293 K. Inset: CW dual-wavelength operation at $\lambda_1=7.46 \mu$ m and $\lambda_2=8.15 \mu$ m with a frequency spacing of 3.4 THz at a current of 1.62 A. (b) THz CW power as a function of current. Inset: CW emitting spectrum at 3.41 THz at a current of 1.62 A.

WPEs of 2.8% and 1% in pulsed mode and CW operations, respectively. [8]

In CW operations, a 4-mm long composite DFB device emits up to 0.53 W with threshold current densities of 1.87 kA/cm², as shown in Fig. 4(a). The inset is the CW lasing spectrum at 1.62 A. Stable dual-wavelength operation at $\square_1=7.46$ \square m and $\square_2=8.15$ \square m with a frequency spacing of 3.4 THz is observed. Golay cell detector (Microtech Instruments) was used for THz power measurement. The power value was not corrected for collection efficiency. Figure 5(b) is the THz power in CW operations at 293 K. Maximum CW power of 14 \square W with conversion efficiency of $\square= 0.35$ mW/W², and THz WPE of 0.8×10^{-6} are obtained. The superlinear increase in CW THz power in Fig. 3(b) is due to the rapid power increase in \square_1 and dramatic power balancing between \square_1 and \square_2 in the current range of 1.451.68 A. The maximum CW power is much higher than previous demonstrations in Ref. 8 despite that the conversion efficiency is lower due to the relatively lower nonlinearity induced by the reduced threshold gain. As a result, the THz CW WPEs are about one order of magnitude higher than that of 0.95×10^{-7} reported in Ref. 8. The increased THz power and WPE are mainly attributed to the enhanced mid-IR power and efficiency by the strongcoupled strain-balanced design. As pointed in Ref. 6, a great portion of the THz light generated within the 4-mm cavity is not outcoupled from the polished facet due to the limited substrate thickness of ~ 340 \square m respect to the cavity length. Ideally, the THz power and efficiency can be further enhanced by a diffraction grating design to vertically extract the THz radiation from the entire cavity. [11]

4. RT-CW MONOLITHIC THZ TUNING

To verify the broadband gain and nonlinearity design of this structure, another sample from the same wafer is processed into a three-section SGDFB-DBR waveguide. Both the two sampled grating (SG) sections are sampled with a very short grating section ($\square_0= 1.22$ \square m, $N_g= 15$) for 7 times. Here N_g is the grating number in one short section. The sampling periods $Z_1=207$ \square m and $Z_2=185$ \square m were used for the front and back SG sections, respectively. To enhance the power performance, the front SG section was further elongated with a 1.5-mm unpatterned section for power amplification. Laser bars with 6.3-mm cavity length were cleaved, containing one 1-mm DBR section ($\square_{DBR}=1.329$ \square m) on the back, one 2-mm SG

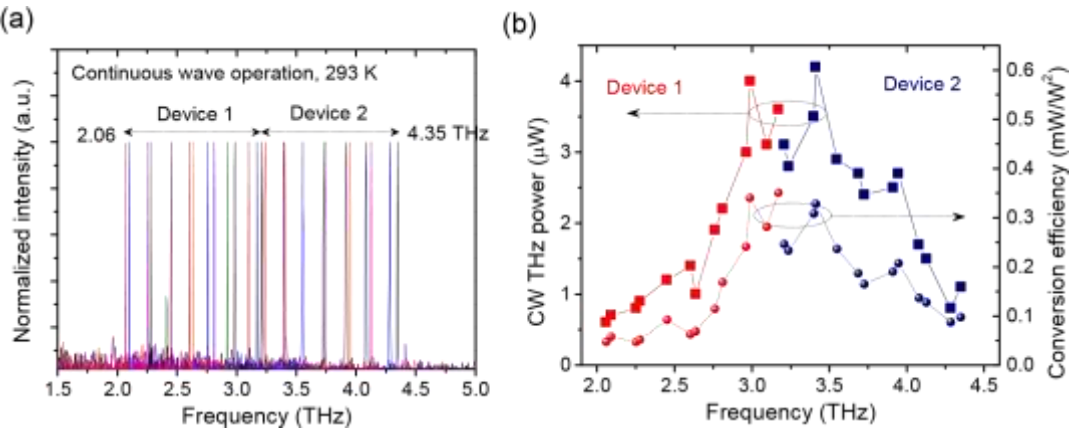


Figure 5 Room temperature continuous wave tuning spectra (a), power and conversion efficiency (b) of the two epi-down mounted THz devices with a combined tuning range of 2.06-4.35 THz.

section (SG1) in the middle, and one 3.3-mm SG section plus the amplifier (SG2) in the front. These three-section devices are then epi-down mounted on patterned diamond submounts for CW measurements.

The measured THz tuning spectra are presented in Figure 5(a). A wide frequency tuning from 2.06 to 3.17 THz with a step of 185 GHz by changing the DC current on SG1, and 2.09 to 3.1 THz with a step of 168 GHz by changing the DC current on SG2, are achieved respectively. Another device with a slightly different grating period designs of $\square_0=1.196 \text{ }\square\text{m}$ and $\square_{DBR}=1.36 \text{ }\square\text{m}$ targeting a larger frequency spacing, exhibits a full tuning range of 3.2 to 4.35 THz, as shown in in Fig. 5(a). The combined tuning ranges for both devices is 2.29 THz. The SMSR ranges from 12 to 25 dB in the tuning range measured with an uncooled farinfrared DTGS detector. In the tuned THz frequencies, the THz output power ranges from 0.6 $\square\text{W}$ at 2.06 THz to 4.2 $\square\text{W}$ at 3.42 THz. The conversion efficiency peaks around 3.0-3.5 THz with $\square_{max}=0.36 \text{ mW/W}^2$ at 3.2 THz, and decreases towards the lower and higher frequency ends, as shown in in Fig. 5(b).

5. CONCLUSIONS

In conclusion, we report a room temperature CW THz source based on a strain-balanced mid-IR quantum cascade laser at 3.41 THz with a SMSR of 30 dB and output power up to 14 μW . The CW THz wall plug efficiency is enhanced by one order of magnitude compared with the previous demonstrations. In addition, the same laser wafer is used to demonstrate room temperature, CW single mode THz emissions with a wide tunable frequency range of 2.06 - 4.35 THz and THz power up to 4.2 $\square\text{W}$ from two monolithic three-section SGDFB-DBR lasers.

6. ACKNOWLEDGMENT

:

This work is partially supported by the National Science Foundation (grants ECCS1306397, ECCS-1505409 and ECCS-1607838), Department of Homeland Security (grant HSHQDC-13-C-00034) “**the published material represents the position of the author(s) and not necessarily that of DHS**”, Naval Air Systems Command (grant N68936-13-C-0124), and an Early Stage Innovations grant from NASA’s Space Technology Research Grants Program. The authors would also like to acknowledge the encouragement and support of all the involved program managers.

References

- [1] M. Razeghi, Q. Y. Lu, N. Bandyopadhyay, W. Zhou, D. Heydari, Y. Bai, and S. Slivken. “Quantum cascade lasers: from tool to product”, Opt. Express, **23**, 8462 (2015).
- [2] Q. Y. Lu, N. Bandyopadhyay, S. Slivken, Y. Bai, and M. Razeghi, “Room temperature single-mode terahertz sources based on intracavity difference- frequency generation in quantum cascade lasers,” Appl. Phys. Lett. **99**, 131106 (2011).

- [3] Y. Bai, N. Bandyopadhyay, S. Tsao, S. Slivken, and M. Razeghi, "Room temperature quantum cascade lasers with 27% wall plug efficiency," *Appl. Phys. Lett.*, **98**, 181102 (2011).
- [4] N. Bandyopadhyay, Y. Bai, S. Slivken, and M. Razeghi, "High power operation of λ 5.2–11 μm strain balanced quantum cascade lasers based on the same material composition," *Appl. Phys. Lett.* **105**, 071106 (2014).
- [5] Q. Y. Lu, N. Bandyopadhyay, S. Slivken, Y. Bai, and M. Razeghi. Widely-tuned room temperature terahertz quantum cascade laser sources based on difference frequency generation. *Appl. Phys. Lett.* **101**, 251121 (2012).
- [6] Q. Y. Lu, N. Bandyopadhyay, S. Slivken, Y. Bai, and M. Razeghi, " Room temperature terahertz quantum cascade laser sources with 215 μW output power through epilayer-down mounting " *Appl. Phys. Lett.* **103**, 011101 (2013).
- [7] Q. Y. Lu, N. Bandyopadhyay, Y. Bai, S. Slivken. And M. Razeghi, "High performance terahertz quantum cascade laser sources based on intracavity difference frequency generation", *Opt. Express*, **21**, 968 (2013).
- [8] Q. Y. Lu, N. Bandyopadhyay, S. Slivken, Y. Bai, and M. Razeghi. Continuous operation of a monolithic semiconductor terahertz source at room temperature. *Appl. Phys. Lett.* **104**, 221105 (2014).
- [9] Q. Y. Lu, S. Slivken, N. Bandyopadhyay, Y. Bai, and M. Razeghi. Widely tunable room temperature semiconductor terahertz source. *Appl. Phys. Lett.* **105**, 201102 (2014).
- [10] Q. Y. Lu, D. H. Wu, S. Sengupta, S. Slivken, and M. Razeghi. Room temperature continuous wave, monolithic tunable THz sources based on highly efficient mid-infrared quantum cascade lasers. *Sci. Reports* **6**, 23595 (2016).
- [11] M. Razeghi, Q. Y. Lu, N. Bandyopadhyay, and S. Slivken, Recent development of high power, widely tunable THz quantum cascade laser sources based on difference-frequency generation. *Proc. of SPIE* **9585**, 958502-1 (2015).